Mem. S.A.It. Suppl. Vol. 24, 61

Memorie della
Supplementi

Granulation in DA white dwarfs from CO5BOLD 3D model atmospheres

P.-E. Tremblay[1], H.-G. Ludwig[1], B. Freytag[2], and M. Steffen[3]

[1] Zentrum für Astronomie der Universität Heidelberg, Landessternwarte, Königstuhl 12, D-69117 Heidelberg, Germany, e-mail: ptremblay@lsw.uni-heidelberg.de
[2] CNRS, Université de Lyon, École Normale Supérieure de Lyon, 46 allée d'Italie, F-69364 Lyon Cedex 7, France
[3] Leibniz-Institut für Astrophysik Potsdam, An der Sternwarte 16, D-14482 Potsdam, Germany

Abstract. Time-dependent 3D simulations of pure-hydrogen DA white dwarf atmospheres have been computed in recent years. Synthetic Balmer lines spectra drawn from these radiation-hydrodynamics (RHD) simulations have been shown to predict surface gravities significantly lower than the standard 1D models, in much better agreement with the expectation that white dwarfs cool at constant mass. We have now computed a grid of CO5BOLD pure-hydrogen 3D model atmospheres for surface gravities from $\log g = 7$ to $\log g = 8.5$ and effective temperatures from 6000 to 13,000 K. Over this range, we observe a significant variation of the intensity contrast of the surface granulation patterns, which indicates the strength of the 3D effects. Furthermore, the size and appearance of granules are also varying considerably. An explanation of these behaviours can lead to a better understanding of the physical processes responsible for the energy transfer in white dwarf atmospheres.

Key words. convection — line: profiles — stars: atmospheres — white dwarfs

1. Introduction

The comparison of the observed and predicted Balmer line profiles has been the most successful method to derive the atmospheric parameters ($T_{\rm eff}$ and $\log g$) of DA white dwarfs (Bergeron et al. 1992; Finley et al. 1997). While hot white dwarfs ($T_{\rm eff}$ > 13,000 K) have a mean spectroscopic mass in the range of 0.61-0.63 $M_{\odot}$ (Tremblay et al. 2011a; Gianninas et al. 2011; Kleinman et al. 2012), cool white dwarfs below $T_{\rm eff}$ < 13,000 K observed in the same surveys show a significant increase of up to 20% in their mean mass. White dwarf stars are expected to cool at constant mass and almost constant radius, hence the increase in mass is likely caused by inaccuracies in the model atmospheres (Tremblay et al. 2010; Koester et al. 2009). Tremblay et al. (2011b) demonstrated that the inability of the 1D mixing-length theory (Böhm-Vitense 1958, hereafter MLT) to properly account for the convective energy transport was the source of the long-standing high-$\log g$ problem. In this first experiment, four 3D CO^{5}BOLD (Freytag et al. 2012) models in a limited range of temperature (12,800 > $T_{\rm eff}$ (K) > 11,300) were computed, and model spectra derived from

Send offprint requests to: P.-E. Tremblay these RHD simulations were shown to predict lower masses than 1D models.

We have recently expanded the CO^{5}BOLD computations to a set of 48 DA model atmospheres in the range of $7.0 < \log g < 8.5$ and $13,000 > T_{\rm eff}$ (K) > 6000[1]. Fig. 1 presents the mass distribution of the SDSS spectroscopic sample (Eisenstein et al. 2006) adopting model spectra either from 1D (Tremblay et al. 2011a) or 3D structures (Tremblay et al. 2013). By relying on 3D spectra, the masses are clearly much more in agreement with the mean mass for hotter radiative white dwarfs (horizontal dotted line in Fig. 1). The 3D models therefore possess a great potential to study white dwarfs, although we are just starting to learn about the physical processes responsible for the differences between mean 3D and 1D atmospheric structures. As an initial step, we look in this work at the spatially resolved emergent intensity and the size of the convective cells. These quantities can not be derived from existing plane-parallel 1D structures and can provide insights on the convective processes in white dwarfs.

We start in Sect. 2 by describing briefly the numerical setup of our CO^{5}BOLD simulations. Then, we characterize in more detail the properties of the surface granulation in terms of intensity contrast (Sect. 3) and characteristic size (Sect. 4) as derived from our RHD models. The conclusion follows in Sect. 5

2. Grid of 3D model atmospheres

Our CO^{5}BOLD simulations rely on the box-in-a-star setup and cover the entire atmospheres ($-5 < \log \tau_R < 3$). The lateral boundaries are periodic, and the top boundary is open to material flows and radiation. The bottom layer is closed to incoming material (but open to radiation) for the 6, 4, 3 and 1 hottest models at $\log g = 7.0$, 7.5, 8.0 and 8.5, respectively. In contrast, the bottom layer is open to convective flows (and radiation) in all other models, and a zero total mass flux is enforced. We adopt a grid of $150 \times 150 \times 150$ points for all models.

[1] We use a step of 0.5 dex in $\log g$ and temperature steps of 500 K (above $T_{\rm eff}$ = 9000 K) and 1000 K (below this temperature).

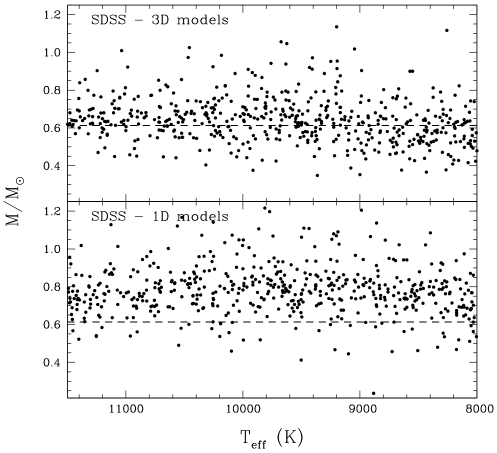

Fig. 1: Mass distribution as a function of $T_{\rm eff}$ for the SDSS sample (S/N > 15) derived from spectroscopic fits using 3D models (top panel) and 1D models (bottom panel). A horizontal dotted lines at the mean mass of the sample ($0.613\ M_\odot$, for $40{,}000 > T_{\rm eff}$ (K) $> 13{,}000$) has been added as a reference.

Details about the input microphysics and numerical parameters will be given elsewhere (Tremblay et al. 2013). We mention, however, that the microphysics is the same as in standard 1D models (Tremblay et al. 2011a). Furthermore, we have verified that the mean 3D structures were not sensitive to variations of the numerical parameters (e.g., size of the boxes and viscosity), unlike the 1D models which are very sensitive to the parametrization of the MLT. In Fig. 2 we present $\langle 3D \rangle$ structures at $\log g = 8$, which are averages in time and space over surfaces of constant Rosseland optical depth, and compare them to 1D structures, adopting the ML2/$\alpha = 0.8$ parametrization of the MLT. There are clearly systematic differences between both physical models of convection. The most striking difference is in the upper part of the atmospheres, where the temperatures are always much smaller in $\langle 3D \rangle$ models, which is the result of convective overshoot. Furthermore, the 1D models feature an abrupt transition from a convective zone to a purely radiative equilibrium at $\tau_R \sim 0.1$, while

3D models are smoother in this region because of convective overshoot.

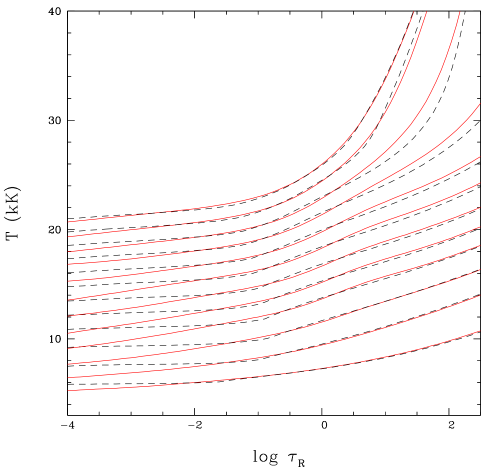

Fig. 2: Temperature structures versus log τ_R for ⟨3D⟩ (red, solid lines) and 1D (black, dashed lines) model atmospheres. From bottom to top, $T_{\rm eff}$ values are from 6000 K to 8000 K (steps of 1000 K) and from 9000 K to 13,000 K (steps of 500 K). The temperature scale is correct for the 6000 K model, but other structures are shifted by 1 kK for clarity.

3. Intensity contrast

The intensity contrast of the surface granulation is one measure of the strength of 3D effects. It must be understood, however, that one can not easily rely on the intensity contrast to predict the resulting 3D effects on the *mean* structures such as those presented in Fig. 2, since local effects may cancel during the averaging procedure. Nevertheless, a study of the granulation properties can provide insights on the physical processes responsible for the formation and evolution of convective cells and in an indirect way, on the energy transfer in the atmospheres. In Fig. 3, we present gray (bolometric) emergent intensity snapshots for 12 of our simulations. For each simulation, we rely on a time average of 250 snapshots similar to those in Fig. 3 to derive quantities presented in this work.

The root-mean-square (RMS) relative intensity contrast is shown in Fig. 4 as a function of $T_{\rm eff}$ (left panel). For all gravities, the intensity contrast resides in the 5-20% range, except for the low and high $T_{\rm eff}$ extremes. This implies that the emergent flux varies significantly over position and time on the disk of these white dwarfs and that the 1D plane-parallel approximation is poor for the resolved atmospheres. Very similar values of the intensity contrast are found for A, F, G and K dwarfs (see Fig. 15 of Freytag et al. 2012). We find that the granulation is visually similar (see Fig. 3) in M dwarfs and ~6000 K white dwarfs, and in A dwarfs and ~12,500 K white dwarfs.

From Fig. 4 (left panel), one could conclude from the shift of the curves at different log g values that the surface gravity has a significant impact on 3D effects. However, when looking at the intensity contrast as a function of the density in the photosphere, (Fig. 4, right panel), the relation becomes much more similar for all gravities. Therefore, the granulation properties appear to be better described by the characteristic photospheric density than the $T_{\rm eff}$ and log g atmospheric parameters. This may also be part of the explanation why the intensity contrast is similar in (hot) white dwarfs and convective main-sequence stars, since the atmospheric densities are of the same order of magnitude.

At the hot end of our grid, the intensity contrast is expected to decrease because the convective to radiative flux ratio becomes very small. At the opposite cool end of our sequence, convection is very efficient to transport the small total flux with only very small temperature variations. In between these two extremes, the increasing total flux contributes to enhance the contrast. Furthermore, as $T_{\rm eff}$ is increasing, the Rosseland opacity is also increasing in the photospheres. This implies lower characteristic densities in the photospheres (see Fig. 4) and higher convective velocities. This effect also contributes in enhancing the fluctuations. The MLT qualitatively account for these effects when predicting the convective velocities.

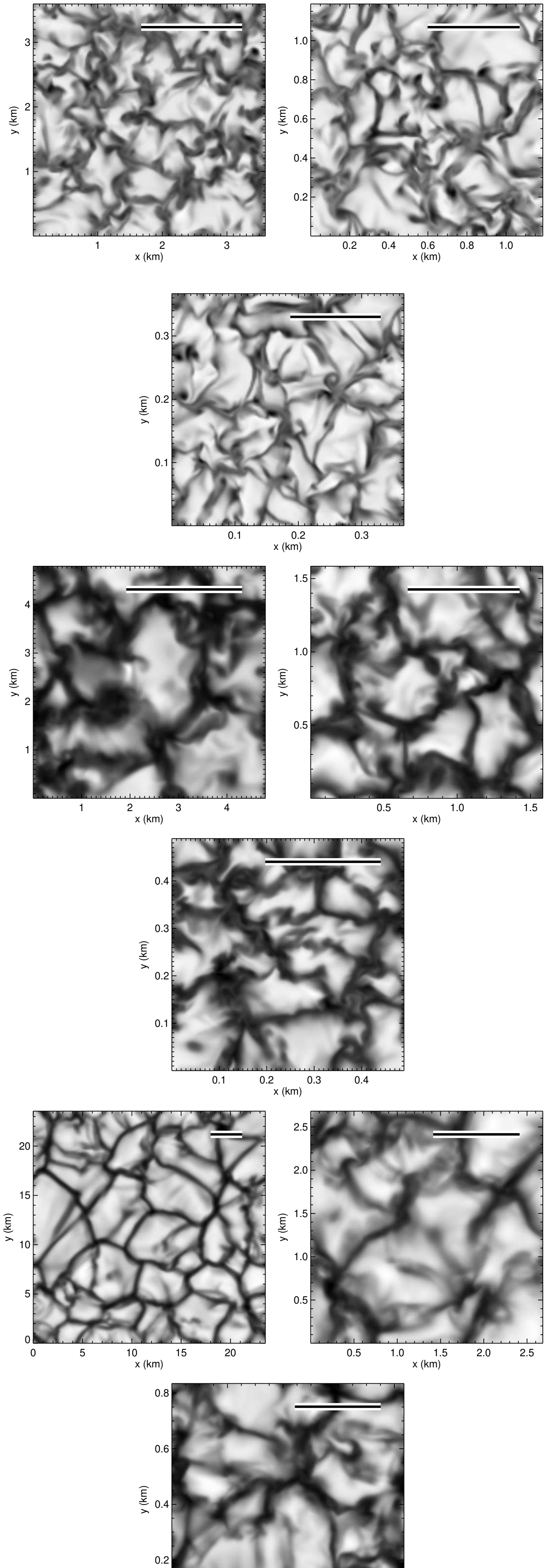
y (km)
x (km)

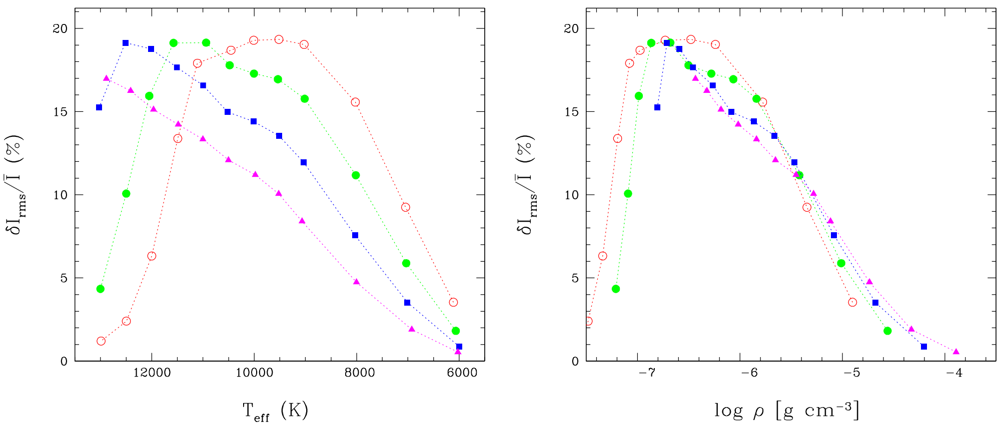

Fig. 4: RMS intensity contrast divided by the mean intensity as a function of $T_{\rm eff}$ (left panel) and $\log \rho$ (evaluated at $\tau_R = 1$, right panel) for our sequence of 3D models at $\log g = 7.0$ (open points, red), 7.5 (filled points, green), 8.0 (squares, blue) and 8.5 (triangles, magenta). The points are connected for clarity.

4. Granulation size

The 3D models have horizontal sizes, while such thing does not exist in 1D plane-parallel models. Calculations of stellar RHD models have shown that granular patterns have larger horizontal dimensions of the order of 10 times the local value of H_p (Freytag et al. 1997). In Fig. 5, we present the power spectrum as a function of the horizontal wavenumber, for the emergent intensity of the 10,000 K and $\log g = 8$ simulation. We did such Fourier transforms for all of our simulations, and we found that the structure of the power spectrum is very similar in all cases.

The maxima of the power spectra are well fitted by a parabola, from which we derived the characteristic size of the granulation as the wavelength of the peak of the power spectrum. We note that this characteristic size is more sensitive to numerical parameters than other quantities derived from our simulations. For instance, we expect that grid resolution and viscosity will have an effect on the size of the granules. Therefore, our values should be taken as estimates only[2].

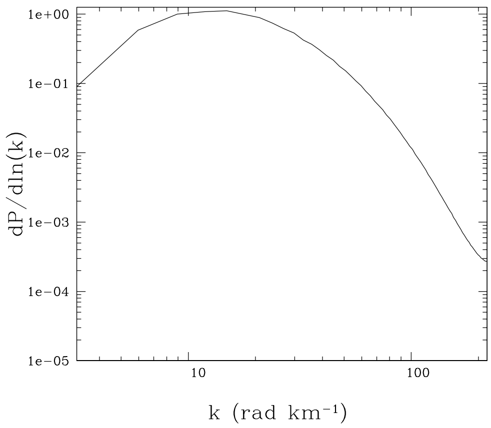

Fig. 5: Mean power spectrum as a function of the horizontal wavenumber ($2\pi/\lambda$) averaged over 250 snapshots of the (bolometric) intensity map of the 10,000 K 3D simulation ($\log g = 8$).

[2] We discard the two hottest models at $\log g = 7$ since convection is too weak to clearly differentiate

The ratio of the characteristic granulation size to the pressure scale height in the photosphere is presented in Fig. 6. It demonstrates that the characteristic cells dimension is not only a function of local the pressure scale height. The size of granules decreases much more rapidly with decreasing $T_{\rm eff}$ than what we would expect from simple thermodynamics considerations.

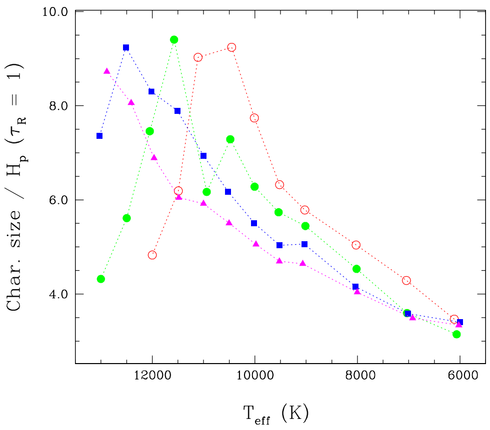

Fig. 6: Ratio of the characteristic granular size (maximum of the mean power spectrum) to the pressure scale height at $\tau_R = 1$ as a function of $T_{\rm eff}$ for our sequence of 3D models. The points are connected for clarity. The color code is the same as in Fig. 4.

The Péclet number in the photosphere ($\tau_R = 1$) which is the ratio of the radiative timescale to the advective timescale (Ludwig & Kučinskas 2012), is shown on Fig. 7. The ratio is changing from a value below to above unity between the hotter and cooler models, respectively. This implies that the evolution of convective cells in the photosphere will be largely influenced by radiation in the hot models in our grid, whereas for the cool models, convective cells are more directly governed by quasi-adiabatic expansion and compression.

granules from the effects of p-mode pulsations and possible unphysical numerical fluctuations.

This effect may be part of the explanation, along with the effect from velocities, for the change in the characteristic size of the granulation. We note that the Péclet number is varying significantly in the photospheres, typically by one order of magnitude or more. Hence the values given in Fig. 7 for one reference layer should be taken as estimates only of the importance of radiative and advective processes in the full photospheres.

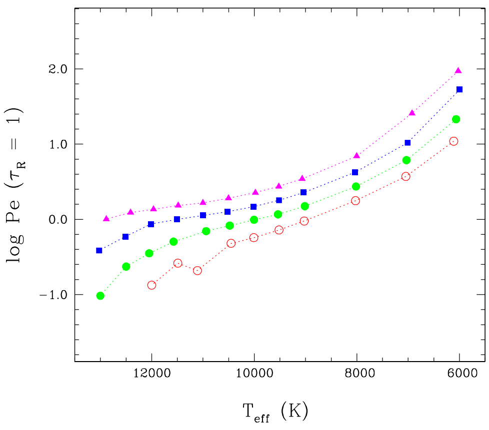

Fig. 7: Logarithm of the Péclet number in the photosphere ($\tau_R = 1$) of our simulations. The color code is the same as in Fig. 4.

Fig. 8 presents a measure of the asymmetry between the dark and bright cells in our simulations, with the surface area fraction occupied by bright cells ($I > \bar{I}$). It is clear that there is a trend for the bright cells to occupy more area in hotter models. This is also seen in the intensity snapshots of Fig. 3, with large bright cells and narrow dark lanes appearing in hot models. This effect can explain in part the increasing characteristic size for hotter models. A similar effect is observed for A-type stars and red supergiants when simulated with CO^{5}BOLD (Freytag et al. 2012). This can be partly attributed to the faster moving downdrafts, that correspond to the small shallow surface granules.

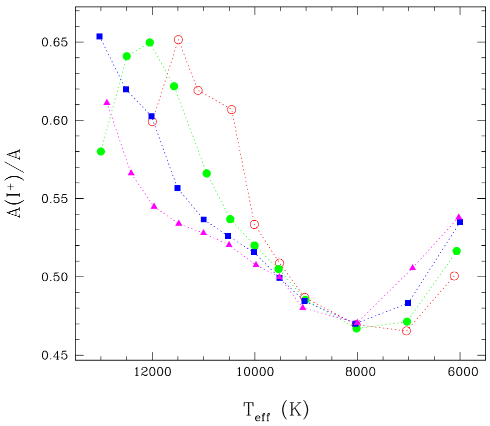

Fig. 8: Fraction of the geometrical surface (A) where the intensity is higher than the average (I^+). The color code is the same as in Fig. 4.

5. Conclusion

We presented a grid of CO^{5}BOLD 3D model atmospheres covering most of the range of observed atmospheric parameters for convective DA white dwarfs down to $T_{\rm eff}$ = 6000 K. We relied on these simulations to look at the properties of the surface granulation. We demonstrated that the emergent intensity contrast is mostly a function of the density in the photosphere, and that granulation in white dwarfs is qualitatively similar to what is observed in the Sun. We have shown that the size of granules is not well scaled by the local pressure scale height, and we believe that this is due to increasing velocities (Mach number) and to the variation of the importance of the radiative versus advective transport of energy. Future works will compare in more details the properties of CO^{5}BOLD simulations for white dwarfs, solar-type stars and giants.

Acknowledgements. P.-E. T. is supported by the Alexander von Humboldt Foundation. 3D model calculations have been performed on CALYS, a mini-cluster of 320 nodes built at Université de Montréal with the financial help of the Fondation Canadienne pour l'Innovation. We thank Prof. G. Fontaine for making CALYS available to us. We are also most grateful to Dr. P. Brassard for technical help. This work was partially supported by Sonderforschungsbereich SFB 881 *The Milky Way System* (subproject A4) of the German Research Foundation (DFG).

References

Bergeron, P., Saffer, R. A., & Liebert, J. 1992, ApJ, 394, 228
Böhm-Vitense, E. 1958, ZAp, 46, 108
Eisenstein, D. J., Liebert, J., Harris, H. C., et al. 2006, ApJS, 167, 40
Finley, D. S., Koester, D., & Basri, G. 1997, ApJ, 488, 375
Freytag, B., Holweger, H., Steffen, M., & Ludwig, H.-G. 1997, in Science with the VLT Interferometer, ed. F. Paresce (New York: Springer), 316
Freytag, B., Steffen, M., Ludwig, H.-G., et al. 2012, Journal of Computational Physics, 231, 919
Gianninas, A., Bergeron, P., & Ruiz, M. T. 2011, ApJ, 743, 138
Kleinman, S. J., Kepler, S. O., Koester, D., et al. 2012, arXiv:1212.1222
Koester, D., Voss, B., Napiwotzki, R., et al. 2009, A&A, 505, 441
Ludwig, H.-G., & Kučinskas, A. 2012, A&A, 547, A118
Tremblay, P.-E., Bergeron, P., Kalirai, J. S. & Gianninas, A. 2010, ApJ, 712, 1345
Tremblay, P.-E., Bergeron, P. & Gianninas, A. 2011a, ApJ, 730, 128
Tremblay, P.-E., Ludwig, H.-G., Steffen, M., Bergeron, P., & Freytag, B. 2011b, A&A, 531, L19
Tremblay, P.-E., Ludwig, H.-G., Steffen, M., & Freytag, B. 2013, submitted for publication in A&A